JOURNAL OF THE MECHANICAL BEHAVIOR OF BIOMEDICAL MATERIALS 55 (2016) 179–190

Available online at www.sciencedirect.com

ScienceDirect

www.elsevier.com/locate/jmbbm

Research Paper

Microstructure, mechanical property and metal release of As-SLM CoCrW alloy under different solution treatment conditions

Yanjin Lu[a], *Songquan Wu*[a], *Yiliang Gan*[a], *Shuyuan Zhang*[b], *Sai Guo*[a], *Junjie Lin*[a], *Jinxin Lin*[a,*]

[a]*Key Laboratory of Optoelectronic Materials Chemistry and Physics, Fujian Institute of Research on the Structure of Matter, Chinese Academy of Sciences, China*
[b]*Institute of Metal Research, Chinese Academy of Sciences, China*

ARTICLE INFO

Article history:
Received 11 July 2015
Received in revised form
20 October 2015
Accepted 23 October 2015
Available online 10 November 2015

Keywords:
CoCrW alloy
Heat treatment
Mechanical property
Metal release
Selective laser melting

ABSTRACT

In the study, the microstructure, mechanical property and metal release behavior of selective laser melted CoCrW alloys under different solution treatment conditions were systemically investigated to assess their potential use in orthopedic implants. The effects of the solution treatment on the microstructure, mechanical properties and metal release were systematically studied by OM, SEM, XRD, tensile test, and ICP-AES, respectively. The XRD indicated that during the solution treatment the alloy underwent the transformation of γ-fcc to ε-hcp phase; the ε-hcp phase nearly dominated in the alloy when treated at 1200 °C following the water quenching; the results from OM, SEM showed that the microstructural change was occurred under different solution treatments; solution at 1150 °C with furnace cooling contributed to the formation of larger precipitates at the grain boundary regions, while the size and number of the precipitates was decreased as heated above 1100 °C with the water quenching; moreover, the diamond-like structure was invisible at higher solution temperature over 1150 °C following water quenching; compared with the furnace cooling, the alloy quenched by water showed excellent mechanical properties and low amount of metal release; as the alloy heated at 1200 °C, the mechanical properties of the alloy reached their optimum combination at UTS=1113.6 MPa, 0.2% YS=639.5 MPa, and *E*%=20.1%, whilst showed the lower total quantity of metal release. It is suggested that a proper solution treatment is an efficient strategy for improving the mechanical properties and corrosion resistance of As-SLM CoCrW alloy that show acceptable tensile ductility.

*Corresponding author. Tel./fax: +86 59163173236.
E-mail address: Franklin@fjirsm.ac.cn (J. Lin).

http://dx.doi.org/10.1016/j.jmbbm.2015.10.019
1751-6161/

1. Introduction

CoCr-based alloys have been widely applied to various types of orthopedic implants such as artificial hip, knee joints, and dentistry due to their excellent mechanical properties and high corrosion resistance. With more and more implants being used in younger patients, the average service life should be extended in order to maintain functional activity (Mitsunobu et al., 2014). Therefore, it is necessary to prolong the longevity to around 25–30 years with the increase in the lifespan of human beings (Mazur et al., 2015; Patel et al., 2012).

In recent years, grain refinement (Yamanaka et al., 2014d), heat treatment (Lashgari et al., 2010), microalloying (Yamanaka et al., 2014c; Yamanaka et al., 2014f), hot deformation (Yamanaka et al., 2014a) etc. have been used to improve the mechanical properties of CoCr-based alloys. Yamanaka et al. (2011) reported that the elongation of Ni-free Co29Cr6Mo alloys increased with reductions in grain size and reaches a maximum when the grain size equals approximately 5.0–10 μm. It was also reported by Yamanaka et al. (2014f) who used a strategy combining microalloying with thermomechanical processing to design CoCrW-based alloys suggested that Si and C as alloying elements caused the brittle σ phase precipitates to be replaced with the plastically deformable Laves phase, resulting in increasing both the alloy strength and the ductility by accelerate the accumulation of lattice defects. Also, a research has been already conducted to improve the room-temperature ductility by control the grain size through hot forging and by adding a nitrogen and carbon element as a substitute element for N to stabilize the γ phase, and the results showed that a tensile ductility of as-cast CoCr based alloy can be achieved mover 30% by increasing the Cr and N contents (Mori et al., 2010). Yamanaka et al. (2014e) used the additions of carbon into the hot-rolled CoCrW alloys to improve the mechanical properties and believed that the strengthening of CoCrW alloys due to added carbon originated from the precipitate of fine $M_{23}C_6$ carbide particles and the coarse carbides caused the gradual decrease in tensile ductility. Otherwise, the metallic implant that exposed in the vivo environment are vulnerable to corrosion and release metal ions (Mitsunobu et al., 2014). The metal ion release, an indicator of the corrosion characteristics of implant devices, in the human body from metal alloys is a major concern in biomedical application (Songür et al., 2009). Thus, it is necessary to determine whether a significant improvement in mechanical property could be obtained without reducing corrosion resistance. In fact, the corrosion characteristics, as well as other properties of the alloy are influenced by its microstructure. Mori et al. (2015) investigated the effects of carbon addition on the microstructure, mechanical properties and metal release of Co29Cr6Mo0.2N. They suggested that the increasing formation of $M_{23}C_6$ reduced the elongation, whilst increased the amount of Co and Cr release during static immersion.

Generally, dental restorations are fabricated by casting and computer-aided manufacturing technologies. However, cast CoCr-based alloys generally exist coarse microstructures and solidification defects as a result of inadequate mechanical properties and inhomogeneous material quality. Hence, their strength and ductility are sometimes lower than practical required. Currently, selective laser melting (SLM) process is considered to be very suitable for biomedical applications due to its ability to build complex shapes of individual implants, such as dentures and bone implants. Basic research on CoCr-based alloys for biomedical applications has been reported using the SLM process. Hedberg et al. (2014) used SLM to build the CoCrMo for dental application. In their investigation, they elucidated that the non-equilibrium microstructure obtained by SLM resulted in a material of higher corrosion resistance from which less amounts of metals were released in the biological fluids compared with a cast CoCrMo alloy. However, the mechanical property is not reported. According to Takaichi et al. (2013), a characteristic SLM microstructure comprising fine cellular dendrites and parallel elongated grains could be obtained; and dense Co29Cr6Mo alloys could exist better mechanical property and lower amounts of metal release when increased higher energy input. In our previous study (Lu et al., 2015), two dense CoCrW alloys were formed by line and island scanning strategy in SLM, and a diamond-network pattern consisting of border structure and square-like structure; SEM showed that the border structure showed the presence of fine homogeneous cellular dendrites with a submicron size, whereas elongated lamellae seem to grow along a direction inside the square-like pattern. Although As-SLM CoCrW alloys with fine cellular dendrites showed adequate yield strength and corrosion resistance, the elongation of the As-SLM condition was relatively low. Thus its insufficient plasticity is now a matter of concern, thereby limited their applications. There is a strong demand to improve the elongation of the As-SLM CoCrW alloys to obtain orthopedic implants with long lifetimes. Generally, the mechanical properties and corrosion resistance can be improved with a short solution treatment by dissolving the large carbide network and produce a more homogeneous structure (Dobbs and Robertson, 1983). Accordingly, improving the properties of the As-SLM CoCrW alloys should be conducted through the application of heat treatments.

To date, compared with the relatively large body of published works on CoCrMo and CoCrW formed by conventional processes, information concerning the effects of heat treatment on the microstructure, mechanical property and metal release of As-SLM CoCrW alloys is scarce in literature. Additionally, microstructures obtained under different solution treatment will response to differing expectation, accordingly resulting in various properties. Therefore, the aim of the present work was the improvement of mechanical properties and corrosion resistance of As-SLM CoCrW alloy with proper solution treatment for biomedical application.

2. Experimental details

2.1. Materials preparation

The commercial CoCrW powders were used to fabricate samples in selective laser melting processing by line scanning strategy according to our previous study (Lu et al., 2015). The average chemical composition of CoCrW powders is listed in Table 1. Therewith the specimens in the study were solution-treated in annealing oven with high purity argon.

The solution treatment temperatures were at 1100 °C, 1150 °C, and 1200 °C for 1 h followed by quenching in water, respectively. As for the 1150 °C, the furnace cooling also applied. The furnace cooling rate was 2.3 °C/min. Finally, the specimens were denominated 1100WC, 1150WC, 1200WC and 1150FC. Table 2 shows the solution treatment plan for As-SLM CoCrW alloys.

2.2. Phase identification and microstructural observation

Specimens with the dimensions of 10 mm × 10 mm × 8 mm for phase and microstructural observation were grinded with water proof emery paper from 240, 600, 800, 1000 up to 1200 grit under running water, then and finally polished with diamond paste. Phase identification was studied by X-ray diffractometer (XRD, D/MAX-2500PC) with CuKα radiation. Microstructural observation was observed using optical microscope (Axio Vert.A1, ZEISS) and Scanning Electron Microscope (SEM, SU-8010) on the surface etched by a mixture of 5 mL H_2O_2 and 20 ml HCl for 10 s at room temperature.

2.3. Mechanical property characterization

Tensile tests were performed on a universal testing machine at room temperature, with an initial strain rate of 2 mm/s. Three specimens were tested for each group. The schematic diagram of tensile specimen is shown in Fig. 1. Fractography were examined by using SEM.

2.4. Static immersion test

The static immersion test was performed in accordance with the ISO 10271 standard. Samples ($n=15$) with the dimensions of 30 mm × 15 mm × 1.5 mm were fabricated by SLM. Prior to performing this study, the samples were ground with water proof emery paper from 240, 600, 800, 1000 up to 1200 grit under running water, then ultrasonically cleaned in acetone for 15 min, rinsed in distilled water and finally dried at room temperature for 3 h. Therewith, the static immersion tests were conducted in 0.9%NaCl. The pH of 0.9%NaCl solution was adjusted to 7.40 by 1% lactic acid. Before test, the polypropylene bottles were carefully cleaned with 5.0 vol% concentrated HNO_3 solution and distilled water to remove impurities referencing to Okazaki and Gotoh (2005). A 10.35 ml of each solution was poured into the polypropylene bottles each containing a plate specimen. All the sealed bottles were placed inside an incubator at 37 °C for 7 d. Also, a 10.35 ml solution without a specimen was also incubated under the same conditions using for the blank test. The concentrations of various metals released into solution were determined by inductively coupled plasma-atomic emission spectroscopy (ICP-AES, Ultima2). Single element standard solutions of Co, Cr and Ni were 1000 mg/L, while W was 10 mg/L (NCS Testing Technology Co., Ltd.). The single element standard solutions of Co, Cr and W were diluted use as the intermediate standard solution (0.1 mg/L, 0.5 mg/L, 1 mg/L and 10 mg/L) to establish calibration curves. The analytical detection limits obtained from calibration curves for Co, Cr, and W were 2 μg/L, 1.5 μg/L, and 0.3 μg/L, respectively. An average of three measurements was taken for each group. The quantity of metal released (μg/cm^2) was estimated using the following formula: The quantity of metal released (μg/cm^2) = [(The quantity of average metal concentration in test solution containing sample) − (The quantity of average metal concentration in blank group)] × 0.01035L/(surface area of specimen).

Table 1 – The chemical composition of CoCrW powders.

	Chemical composition (mass %)								
Co	Cr	W	Si	Mn	C	N	Fe	Ni	Be
Bal.	28.00	9.00	1.50	≤0.01	≤0.05	≤0.002	≤0.05	/	/

2.5. Statistical analysis

The SPSS15.0 statistical software package was used for data analysis. $P>0.05$ was considered as no statistically significant difference.

3. Results

3.1. Phase analysis

Fig. 2 shows the XRD pattern of the CoCrW alloys with and without heat treatment. Apart from the 1200WC, it can be found that the diffraction peaks belong to face-centered cubic

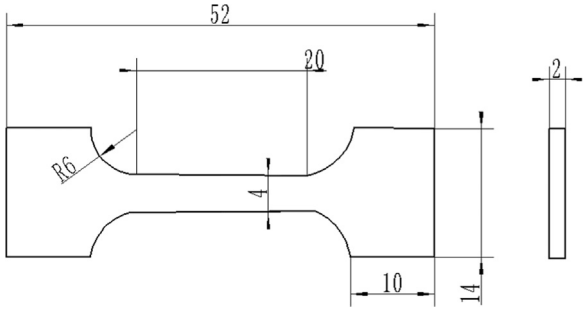

Fig. 1 – The schematic diagram of tensile specimen.

Table 2 – The solution treatment plan for As-SLM CoCrW alloys.

Number	1	2	3	4	5
Temperature/time	As-SLM	1100 °C/1 h	1150 °C/1 h	1200 °C/1 h	1150 °C/1 h
Cooling	/	WC	WC	WC	FC
Denominated name	As-SLM	1100WC	1150WC	1200WC	1150FC

WC= water quenched; FC= furnace cooling

(fcc) γ and hexagonal close-packed (hcp) ε phases of Co were detected in As-SLM, 1100WC, 1150WC and 1150FC specimens, among which some differences of intensity can be observed. For As-SLM alloy, the intensity of peaks of the γ and ε phases was relative strong. However, the intensity of γ and ε became strongest after heating at 1150 °C with furnace cooling. Moreover, the peak of σ phase was also detected in the 1150FC alloy. In contrast, the intensity of peaks of γ displays a remarkable decrease with the increase of the treatment temperature from 1100 °C to 1200 °C when the water quenching was applied. It is clearly in 1200WC that the γ phase drops nearly to zero when heated at 1200 °C, while 1100WC and 1150WC alloys shows duplex phases of γ and ε phases. Apart from γ and ε, no significant degree of the other peaks can be observed in 1100WC, 1150WC and 1200WC alloys.

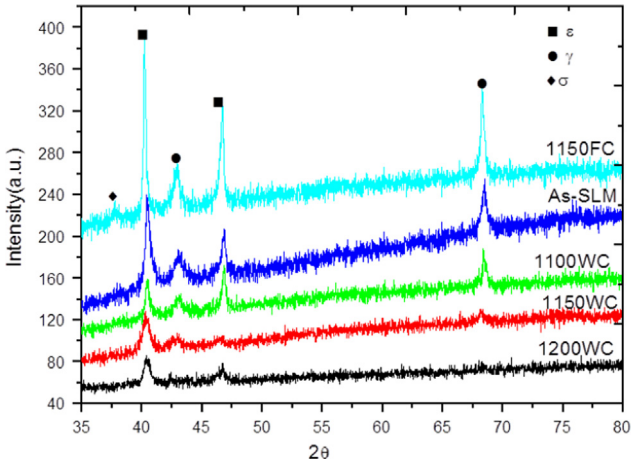

Fig. 2 – XRD patterns of the CoCrW alloys with and without solution treatment.

3.2. *Microstructure analysis*

Fig. 3 presents the optical micrograph (OM) of the As-SLM CoCrW alloys heated at different conditions. The As-SLM alloy appears distinctive diamond-like network pattern consisting of border structure and square-like structure as denoted by white lines in Fig. 3a. The 1150FC alloy heated at 1150 °C with furnace cooling shows the presence of an amount of precipitate and diamond-like network pattern (Fig. 3b). When alloy heated at 1100 °C following water quenching, the microstructural feature is similar to the 1150FC alloy, but the morphology of precipitates changes from large size into tiny ones (Fig. 3c). However, solution treatment at 1150 °C and 1200 °C following the water quenching results in a complete disappearance of diamond-like network pattern (Fig. 3d and e).

Fig. 4 displays the backscattered electron images (BSE) of the As-SLM CoCrW alloys heated at different conditions. It is evident in Fig. 4a that the As-SLM alloy shows a much finer structure and non-equilibrium structure. In addition, it is noted that some ε martensite phase is identified as striations within grains in the As-SLM. As treated at 1150 °C following the furnace cooling, a dense and large amount of bright blocky precipitates is randomly dispersed inside the grain or at the grain boundaries; In the case of water quenching, the microstructure of 1100WC alloy shows a distribution of very fine precipitates within the grain and at the grain boundary. In contrast, similar microstructure consisting of fine grain structure with annealing twins and a spot of tiny black precipitates inside the grains can be observed in the 1150WC and 1200WC alloys after the solution treatment at higher temperature. According to the literature (Chen et al., 2014; Zangeneh et al., 2012), it is expected that the tiny black precipitates is $M_{23}C_6$. The annealing twins observed in

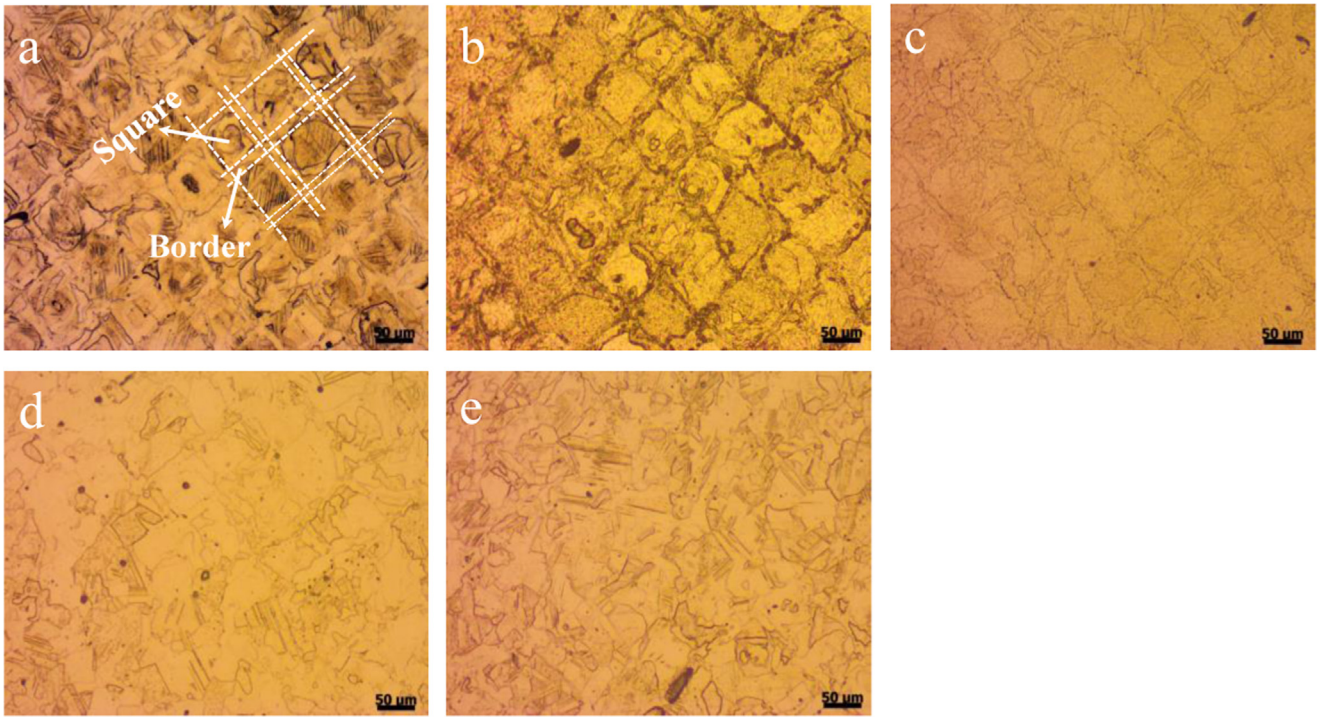

Fig. 3 – OM images of the CoCrW alloys: (a) As-SLM, (b) 1150FC, (c) 1100WC, (d) 1150WC and (e) 1200WC.

the 1150WC and 1200WC suggested that martensite transformation from the γ-phase to the ε-phase occurred during cooling to room temperature (Yoda et al., 2012).

Fig. 5 shows the EDS patterns of the precipitates in the SEM images of 1100WC and 1150FC alloys. From the EDS pattern, the bright particles in the1100WC (Fig. 5a) and

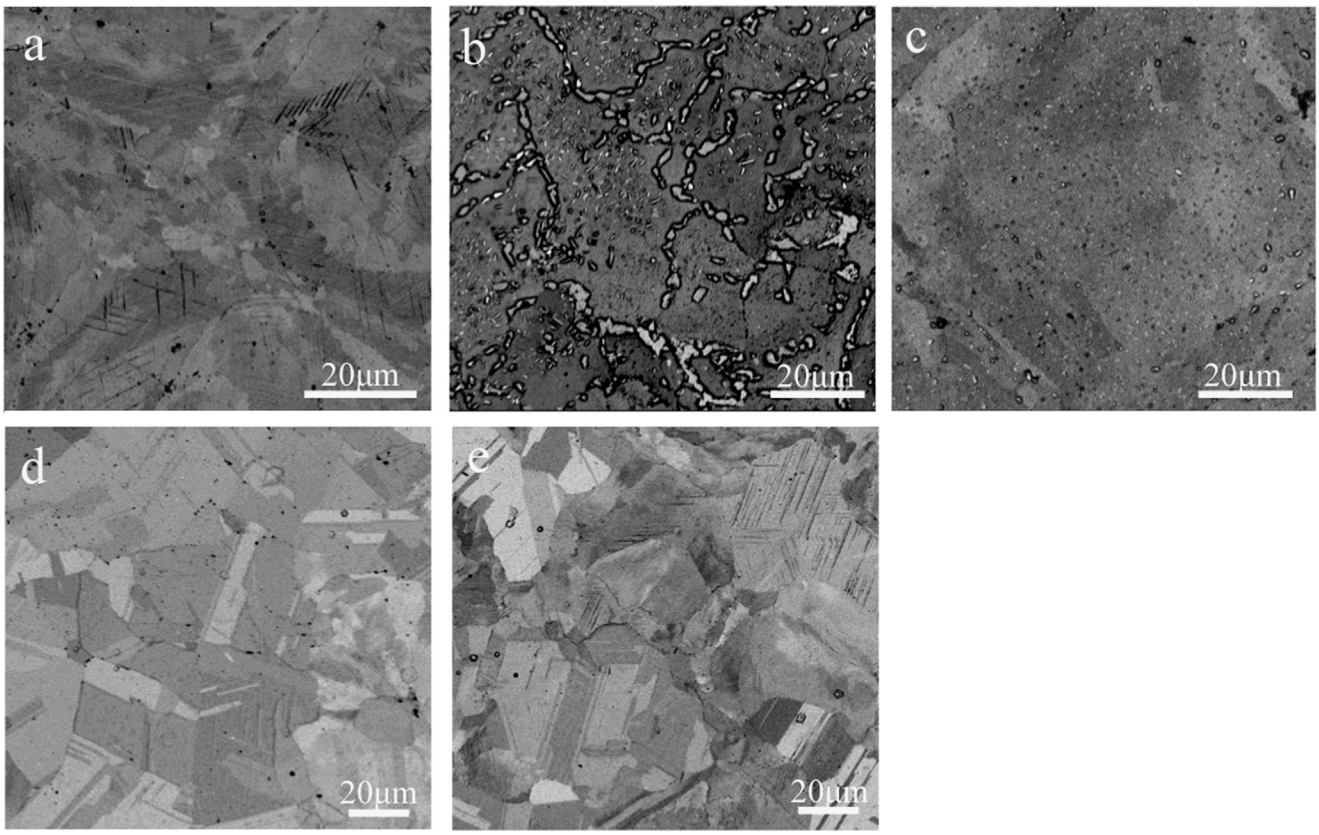

Fig. 4 – BSE of the alloys: (a) As-SLM, (b) 1150FC, (c) 1100WC, (d) 1150WC, and (e) 1200WC.

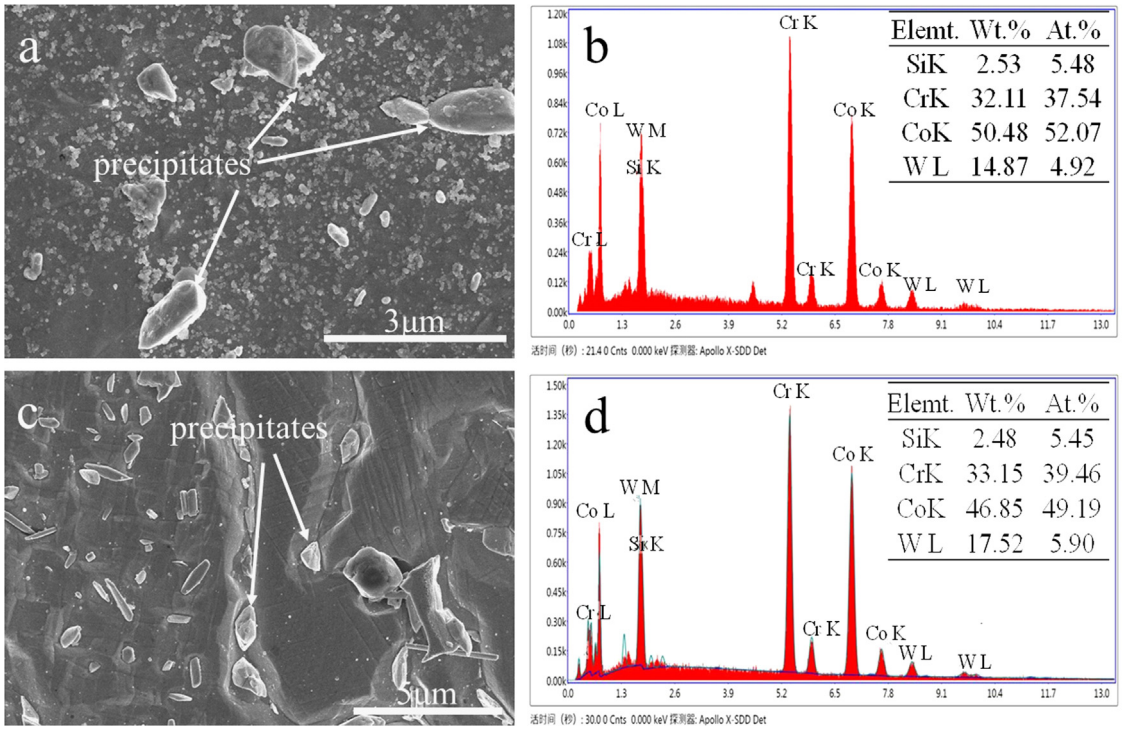

Fig. 5 – EDS patterns of the precipitations (b–d) in the SEM images of 1100WC (a) and 1150FC (c) alloys.

1150FC (Fig. 5c) alloy are main composition of high Si, Co, Cr, and W. The quantity of Co is lower than that of the matrix, whilst the Cr content is higher that of the matrix. According to the previous results on the chemical compositions of the precipitations, i.e., the Laves-, σ- and $M_{23}C_6$-phases, the particles should not the Laves phase particles, because the concentration of Cr in the particles is higher than that of Cr in the surrounding matrix (Yamanaka et al., 2014b). Also the $M_{23}C_6$-phases should be excluded, because the $M_{23}C_6$ is Co-depleted and Cr-rich phase. Therefore, it can be confirmed that the precipitates at the grain boundaries is identified as σ phase (Narushima et al., 2013); according to Yamanaka et al. (2014b), the σ phase is identified in the alloys at low-carbon concentrations of 0.01 mass%, which is identical to the alloy in our present study.

3.3. *Mechanical property*

Fig. 6 shows the stress–strain curves of tensile test specimens and the mechanical properties. As can be seen from the Fig. 6a, no characteristic of macroscopic necking is observed in all the tensile specimens. The mechanical properties of specimens are listed in Table 3 and Fig. 6b and c. The As-SLM alloy exhibits the highest ultimate tensile strengths (UTS) and 0.2% yield strengths (0.2%YS), respectively along with elongation of 9.8%. It can be found that the elongation-to-failure of the As-SLM CoCrW alloys significantly depended on the heat temperature and cooling rate. As for water quenching, the UTS and elongation increased with the solution temperature, while there is no significantly difference in 0.2%YS of alloys (Fig. 6b–d). When increased the heat temperature, the elongation increased from 15% to 20%; as heated at 1200 °C, the 1200WC alloy displays the highest elongation of 20%. Additionally, the different cooling ways lead to the differing mechanical properties. Compared with the 1150WC using the water quenching, the 1150FC alloy cooled in furnace shows a marginal increase in UTS and 0.2%YS. However, considerable drop occurred in elongation (Fig. 6d).

Table 3 – The mechanical properties of specimens.

Samples	UTS (MPa)	0.2%YS (MPa)	E (%)
1100WC	1026±3.0	651.0±7.0	15.0±0.34
1150WC	1035.5±2.5	654.5±10.7	17.5±1.25
1200WC	1113.6±9.2	639.5±7.6	20.1±0.5
1150FC	825.18±7.5	593.2±11.7	4.80±0.90
As-SLM	1158.22±21.0	850.0±23.0	9.80±0.10

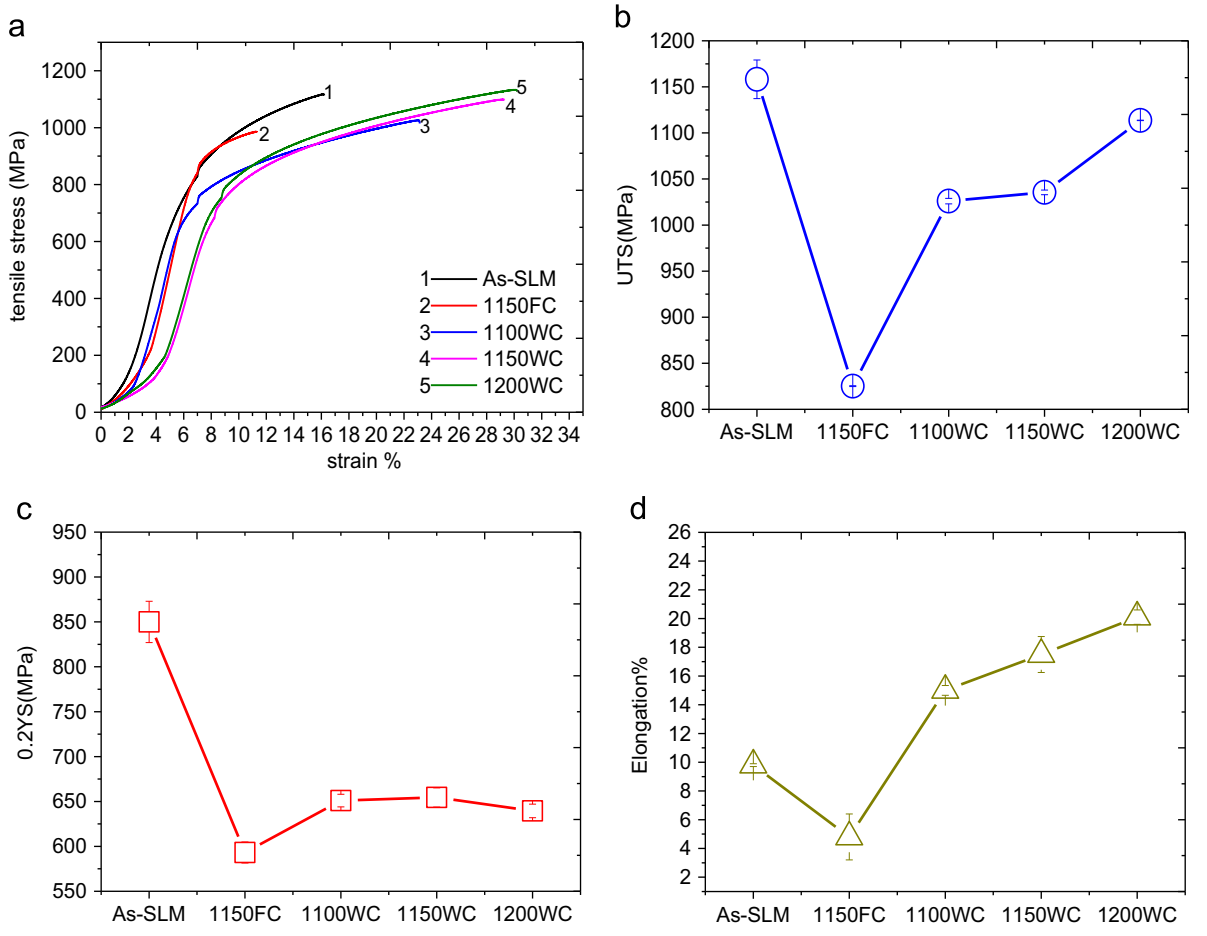

Fig. 6 – Stress–strain curves (a) of tensile test alloys with and without solution treatment and the tensile properties, (b) UTS, (c) 0.2%YS and (d) elongation.

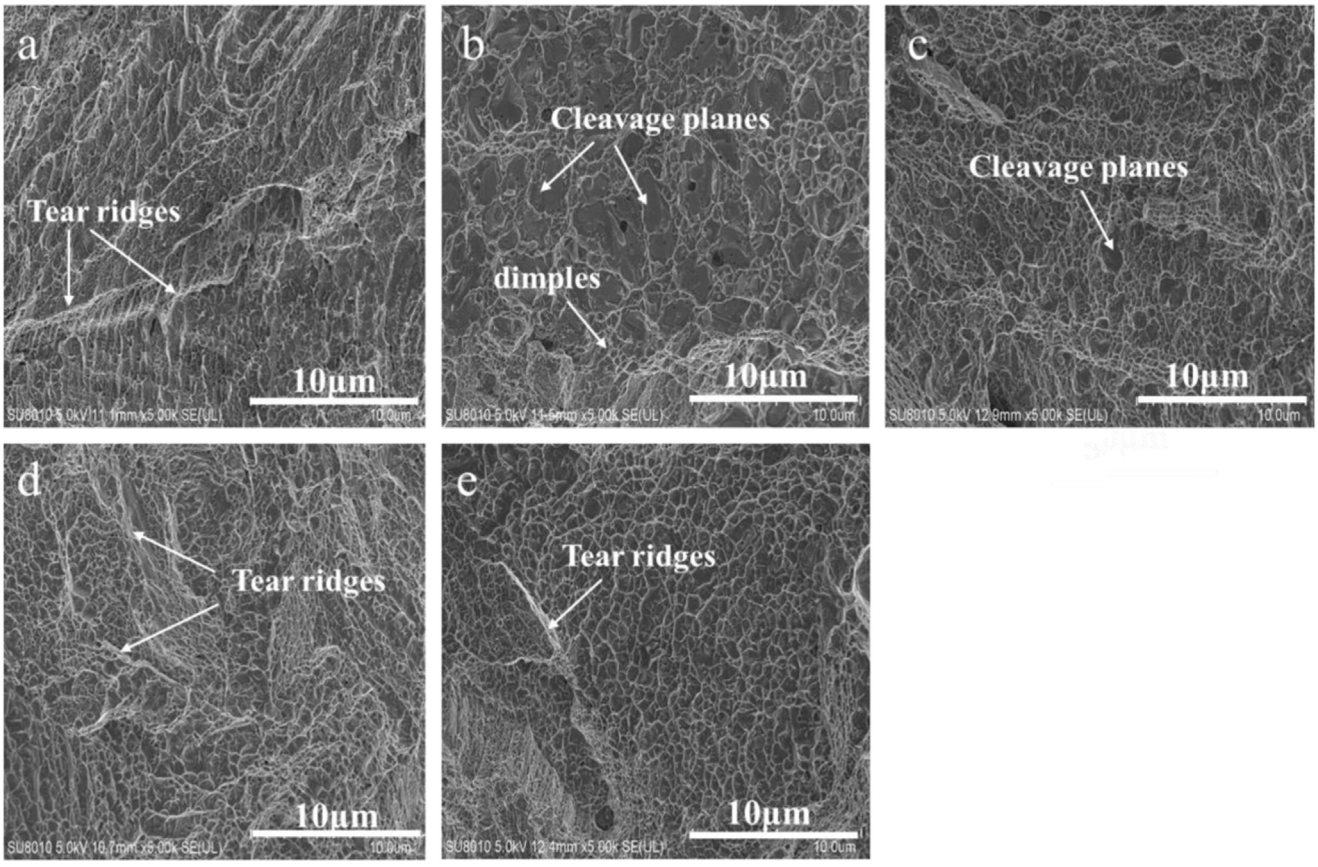

Fig. 7 – SEM images of the fracture surface after tensile test: (a) As-SLM, (b) 1150FC, (c) 1100WC, (d) 1150WC, and (e) 1200WC.

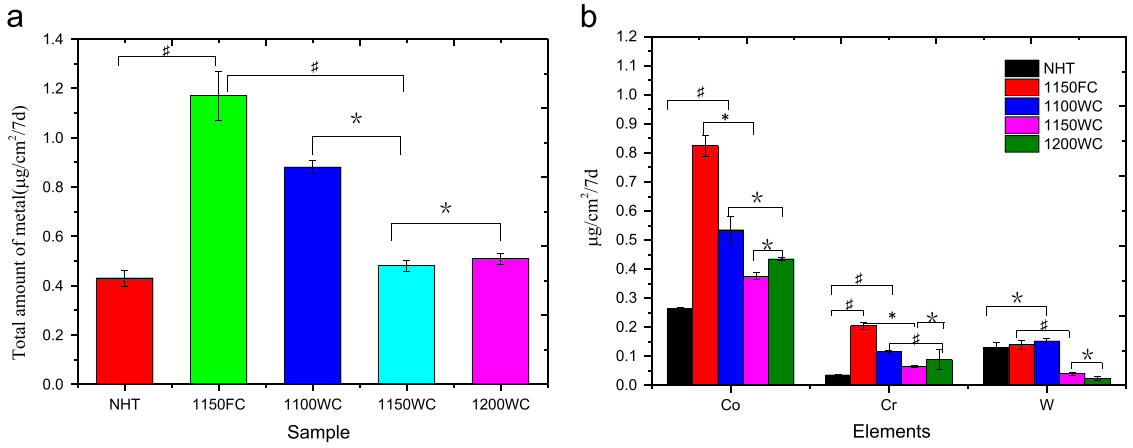

Fig. 8 – Metal release of CoCrW alloy immersed in 0.9%NaCl solution for 7 days (♦Significant at $P>0.05$; *Significant at $P<0.05$; ♯Significant at $P<0.01$).

Fig. 7 demonstrates the SEM fracture surface of As-SLM CoCrW and ones under different solution treatment conditions. For the As-SLM alloy, the fracture appearance appears mainly as tear ridges with a little dimples (Fig. 7a). As indicated in our previous study, the fractured mechanism of the As-SLM alloy was recognized as quasi-cleavage-type fracture (Lu et al., 2015). For the 1150FC alloy in Fig. 7b, the fracture surface mainly appears smooth cleavage planes, indicating a typical brittle fracture behavior of the poor ductility, although little and shallow dimples are also identified. After the solution treatment at 1100 °C following water quenching, the improved ductility lead to the quasi-cleavage characterized as a mixture of the small cleavage planes and shallow dimple-like patterns (Fig. 7c). However, dimples become dominant in the fracture surfaces, where shows much less cleavage planes. When the heat treatment increased to 1150 °C and 1200 °C, the fracture surfaces of 1150WC and 1200WC alloys are distributed by fine dimples with long tear ridges (Fig. 7d and e), indicative of a highly ductile fracture. The dimple features suggests that the voids

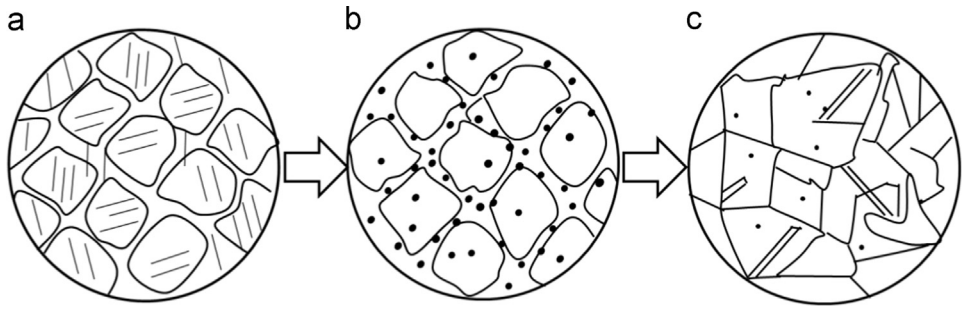

Fig. 9 – Schematic illustration of the microstructural change of As-SLM alloy during solution treatment.

were initiated around the precipitates, and their growth and coalescence led to fracture (Sun et al., 2014). The ductile fracture is corresponding to the characteristics of an intermediate ductile fracture mode.

3.4. *Metal release*

Fig. 8 shows the results of metal release of the CoCrW alloys immersed in 0.9%NaCl solution for 7 days. Error bars in the figure show the standard deviation. The total released metals (Co, Cr and W) ranked by the following order: 1150FC > 1100WC > 1200WC > 1150WC > As-SLM, seen Fig. 8a. Regarding the individual metal shown in Fig. 8b, it is evident that the total quantity of metal element released from the 1150WC alloy is highest than the other samples. For the Co element, Co is more active than Cr and W independent of solution temperature. It is noted that the Co represents in most cases above 60% of the total metal ion release for each sample independently on the solution temperature. This indicates that Co is preferentially released from CoCrW alloy. The As-SLM sample shows the lowest the amount of Co, while the 1150FC sample released the highest amounts of Co ($p<0.01$); meanwhile, the quantity of released Co in 1150FC cooled in furnace is approximately twice higher than that in 1150WC quenched by water ($p<0.05$). The similar trend is also observed in the amounts of released Cr. When coming to the W element, the amount of released W is strongly reduced after 1150 °C and 1200 °C solution treatment following water quenching when compared with the other treatment ($p<0.01$). Furthermore, no Ni ions were detected in the immersed solution.

4. Discussion

4.1. *Phase*

As shown in XRD pattern (Fig. 2), a large amount of γ phase was maintained as a metastable phase at room temperature in As-SLM alloy. The martensite ε phase was induced by the transformation of γ phase to the martensite ε phase when the previous solidified layers were reheated and remelted by the subsequent layer under the quick cooling rate during the SLM process (Lu et al., 2015). Generally, CoCr-based alloys undertake a phase transformation from γ phase to the martensite ε phase during the cooling process, and a large amount of ε martensite are produced after water quenching from temperature above 1100 °C (Huang and Lopez, 1999; López and Saldivar-Garcia, 2007; Saldivar-Garcia and Lopez, 2004). After the solution treatment, the 1150FC, 1100WC, and 1150WC alloys exhibited duplex γ and ε phase, but nearly full ε phase in the 1200WC. This indicates that the fractions of γ and ε phases strongly depend on temperature and cooling method. Since the γ phase was identified in the initial microstructure of As-SLM, the partial ε-phase must originate from the γ→ε martensitic transformation during cooling process. It is noted that the 1150FC alloy coexisted with largest fractions of duplex phases comprising γ and ε after the furnace-cooled; but the amount of γ phases decreased, whilst the ε phase became dominant as heated above 1100 °C following the water quenching. Apparently, a large amount of the formation of ε martensite was strongly favored at high cooling rates from a higher temperature. It is evident that a few γ phases observed on the 1100WC and 1150WC alloys; in contrast, the peaks of the γ phase are hardly visible in 1200WC alloy after solution treatment at 1200 °C with water quenching. This means that the nearly complete γ→ε phase transformation equilibrium temperature can be estimated to be approximately above 1200 °C. Moreover, this transformation of γ→ε phase was also owning to more internal stresses generated by the water quenching from higher temperature of 1200 °C, which would promote the partial γ→ε transformation (Lashgari et al., 2010).

4.2. *Microstructure*

Before considering the mechanism property and metal release, the formation of microstructure and precipitation at different solution treatment condition should be elucidated. Fig. 9 shows the schematic illustration of the microstructural change of As-SLM alloy during solution treatment. As can be seen from the BSE images in Fig. 4, disparity of the microstructure and the amount of precipitate phases were formed in the alloys. Actually, the formation of the diamond-like network structure with dense striations in As-SLM alloy has been investigated in our previous study (Fig. 4a and Fig. 9a), which was never observed before in traditional CoCr-based alloys(Lu et al., 2015). The large amount of striations in As-SLM alloy may be attributed to a large nucleation of ε-embryos promoted by lattice defect formation during the rapid cooling in SLM processing (Barucca et al., 2015). It is considered that the overlapping regions existed highest residual stress. This is because when subsequent laser tracks

was processing, the prior overlapping melted tracks were remelted by the subsequent laser tracks during the SLM, thereby suffered quenching-like processing, resulting in the high residual stress in the overlapping region (Zhang et al., 2005). Liu (2011) showed that the residual stress in the overlapping region was higher than that of the interior region of a single pass. It is reasonable that the precipitates preferentially precipitated in overlapping region due to higher energy from the residual stress during heat treatment while the alloys undergo continually recrystallized; when solution at 1100 °C following the water quenching, the diamond-like structure with the dispersion of the small precipitates still presented in 1100WC alloy (Fig. 9b). It is noted that a fine microstructure with random crystallographic orientations and small tiny carbide was identified (Fig. 9c) when solution at 1150 °C and 1200 °C following the water quenching. More importantly, the diamond-like pattern was not visible at these conditions (Fig. 8c). The findings regarding the microstructure change and precipitate behavior in 1150WC and 1200WC alloys is related to matrix element diffusing and carbon dissolving into matrix phase at high temperature, thereby promoted the grain boundary migration and recrystallization. Compared with the water quenching, the microstructure with coarse and continuous precipitates in 1150FC have important implications for the cooling rate that the furnace cooling provides sufficient time for the phase precipitating.

4.3. *Mechanical property*

As-SLM CoCrW alloy showed highest strengths including UTS and 0.2%YS, but non-ideal elongation for surgical application. As described in Introduction, the elongation of the As-SLM condition was probably due to the diamond-network microstructure with dense striation to some extent. The high strengths of As-SLM alloy should be related to the striation consisting of residual γ phase and ε phase, seen Fig. 4a; such striations would impede the dislocation glide operative in γ phase through the martensite ε phase with dense stacking faults, and enhance a high stress concentration at γ–ε interfaces where tend to become sites of crack initiation and propagation during tensile deformation. On the other hand, striation grown on the {111}γ planes that restricts the dislocations slip in the γ-phase (Koizumi et al., 2013; Lee et al., 2005). As a consequence, a premature fracture before sufficiently uniform elongation occurs.

Therefore, it is necessary to improve the mechanical properties of As-SLM CoCrW alloy by heat treatment to dissolve the diamond-like network structure and thereby recrystal a more homogeneous one. Results from the tensile test suggest that the expected mechanical properties of the As-SLM CoCrW alloy can be controlled by recrystallization under optimal heat treatment conditions. There is no doubt that it should describe the correlation between the microstructure change and mechanical properties under different conditions. It is well accepted that if the precipitates appeared constitution type, they would accordingly result in loss of the desired properties. Previous study indicated that microstructure containing a dispersion of σ phase particles would result in inferior ductility (Rosenthal et al., 2010). Liao et al. (2012) considered that the spherical and discontinuous island carbide structure can increased ductility, whereas the coarse carbides are detrimental ductility. The coarse and dense precipitate dominantly is detrimental to the elongation, which cause stress concentration and crack initiation and lead to the growth of microvoids as a result of an insufficiently fracture (Yamanaka et al., 2014e). There is a high probability that the fractures of the 1150FC alloy much be triggered by the coarse precipitates located at the grain boundary regions (Fig. 4b). In contrast, the distribution of small and fine precipitates inside the grain or grain boundary (Fig. 4c), the ductility of the 1100WC alloys were significantly increased to 15%.

Regarding the 1150WC and 1200WC, despite they existed large fraction of the ε martensite in XRD pattern (Fig. 2), reversely showing excellent elongation, especially for 1200WC. This seems not agree with the previous conclusions that CoCr-based alloy with γ phase structure exhibited better ductility due to the former having a relatively large number of effective slip systems; while the amount of ε martensite phase greatly was known to reduce the ductility due to ε martensite plates would introduce a high stress concentration at their interfaces and/or grain boundaries, resulting in premature fracture before the onset of plastic instability (Lee et al., 2007). For example, Yamanaka et al. (2014e) reported that the amount of ε martensite phase that forms due to athermal martensitic transformation greatly reduced the ductility of CoCrMo alloys. Yoda et al (Yoda et al., 2012) who investigated the effects of Cr and N content on the microstructures and mechanical properties found that elongation of CoCrMo alloy increased with peak intensity of the ε phase decreased. However, a higher strength and a similar excellent elongation of 20.1% were obtained in 1200WC alloy with the present of nearly full ε martensite. It was reported that the presence of athermal ε martensite enhanced the quasi-cleavage type fracture due to the stress concentration occurred when strain-induced martensite ε phase intersected with the preexisting athermal ε martensite (Yamanaka et al., 2011). However, in the study since the matrix phase had already transformed to a nearly full ε phase, no strain-induced martensitic transformation (SIMT) was possible. Therefore the SIMT certainly would not propagate along the interface between the γ phase and the SIMT ε phase on {111} to form a quasi-cleavage fracture (Sun et al., 2014). This analysis is corresponding to the characteristics of an intermediate ductile fracture mode (Fig. 7). Although, it is accepted that fine carbide precipitates in intragranular regions contribute to increase the strength due to the micro-voids can initiate around the precipitates as a result of large plastic deformation, the remarkable improvement of elongation should not be interpreted simply in the context of the precipitation behavior. Herein, this result should not completely attribute to the distribution of small and fine precipitates inside the grain or grain boundary that reinforce the matrix in the case. There should be the other factors endowing the excellent ductility. Thus, a large numbers of the dislocations on the basal plane in the water quenched alloys may be considered (Sun et al., 2014). According to the research from Matsumoto et al. (2014), a polycrystalline CoCrMo alloy consisting of a single ε hcp structure without

σ precipitates also exhibited both high strength along with an excellent plastic elongation at room temperature, in spite of the relatively limited number of slip systems due to the present of martensite ε phase. They elucidate that the simultaneous activation of both the basal ⟨a⟩ slip and prismatic ⟨a⟩ slip was noted, which should responsible for the excellent elongation. Therefore, the dominant deformation mode of the nearly full ε phase CoCrW alloys may be due to simultaneous activation of basal ⟨a⟩ slip and prismatic ⟨a⟩ slip. Nevertheless, as the detail mechanisms involved remain unclear the associated basal ⟨a⟩ slip and prismatic ⟨a⟩ slip should be further investigated.

4.4. *Metal release*

The metal release in the biological environments is an indicator of the corrosion characteristics of a biomedical alloy, which is closely linked to their corrosion resistance and mechanical property. The metal release results in Fig. 8 show the released concentrations of Co, Cr, and W were affected by solution temperature and cooling method. The difference in metal release should be attributed to the distinct microstructure and phase. There are some factors should be taken into account for explaining the metal release behavior. On one hand, when corrosive solution arrived at the substrate, the initial metal release may be attributed to the dissolution of unstable precipitates in the surface oxide until the formation of passive surface oxide. On the other hand, it is considered that the presence of grain boundaries and precipitates may cause the selective corrosion. Bettini et al. (2012) who investigated the influence of grain boundaries on the dissolution behavior of a CoCrMo alloy in phosphate buffer saline solution by scanning Kelvin probe force microcopy found that metal release initiated from the matrix areas around carbides and grain boundaries. This may due to the depletion of Cr, Co and W around the precipitates, which contained richer Cr, Co and W than matrix. Given this, metal release preferentially occurred around the precipitates. That is, the more number of precipitates and grain boundaries that formed by the precipitates, the more initiation sites for metal release. Interestingly, it can be found that the amount of W release of 1150WC and 1200WC dramatically reduced when compared with other specimens. It is conjectured that W release behavior can be inhibited in the ε hcp structure to some extent. When compared with the 1150WC and 1200WC alloys, the fact is that the 1150WC alloy shows slightly less metal release than that of 1200WC one. More internal stresses generated from the water quenching from higher temperature of 1200 °C should be responsible for the behavior (Lashgari et al., 2010). In view of above analysis, the internal stresses may be used to explain that why the amount of the 1150WC was lower than that of 1200WC. It has been widely proved that the excellent corrosion resistance of CoCr-based alloy results from a Cr-rich passive surface oxide on the substrate in most biological environments (Jacobs et al., 1998; Okazaki et al., 1997). Okazaki et al. (1997) who used XPS examination the passive films formed on 316 L stainless steel and CoCrMo alloy in a calf serum solution, elucidated that the amount of metal release depended on the Cr content in the oxide film. Actually, the precipitates can act as preferential initiation sites for the breakdown of passive film (Zhang et al., 2014). On the basis of the considerations, this also may be used to explain that why the amount of the 1100WC and 1150FC was larger than that of the other groups. Further study is needed to investigate the cytotoxic reactions of the CoCrW alloy.

The daily dietary intake of Co, Cr, and Ni is 250, 240, and 400 μg, respectively (Geurtsen, 2002). Co, Cr and Ni release can be cause clinical failure or cutaneous allergic reactions (Summer et al., 2007), which is related with the clinical implant failure of artificial joint prostheses (Okazaki and Gotoh, 2005). It has been reported by Anissian et al. that Co ions would effect on human osteoblast proliferation and collagen synthesis when Co concentrations was above 10 μg/mL in the cell culture medium (Anissian et al., 2002). The Cr is most probably released as Cr^{3+}, and it is demonstrated that Cr^{3+} ions would induce cell mortality (Fleury et al., 2006; Hedberg and Odnevall Wallinder, 2014). Regarding Ni, the rate of Ni release should be not more than 0.2 μg /cm^2/7 d into artificial saliva solution (Okazaki and Gotoh, 2008). In the study, the quantities of weekly Ni releases from heated CoCrW alloy into 0.9% NaCl were 0 μg /cm^2/7 d. For W element, in vivo experimental and in vitro studies have been conducted to determine metabolic and toxicity profile of W, which is not considered very toxic for humans (van der Voet et al., 2007).

It has to be mentioned that mechanical property will be reduced when implants suffer corrosion in vivo environment under mechanical loading conditions. Therefore, in further studies the releationship between the metal release behavor and mecahnical change with cyclic load condition should be investigated. Also, the surface modification of the CoCrW alloy will be considered to increase its biocompatibility and longevity of implants.

5. Conclusions

In the present study, the microstructure, mechanical property and metal release of As-SLM CoCrW alloys under different solution treatment conditions were systemically investigated. Within the limitations of this study, the main results obtained can be listed as follows:

1. The microstructure and precipitates in the CoCrW alloys depended on the solution temperature. The diamond-like structure and amounts of precipitates could be observed in the alloys heated at 1100 °C with water quenching and 1150 °C with furnace cooling. At higher temperatures, such as 1150 °C and 1200 °C after water quenching, the diamond-like structure was completely vanished and the amount of precipitates was almost reduced. Thus, a proper solution treatment can cause the precipitate dissolution into matrix and elimination of the grain boundary precipitates.
2. The mechanical properties of the CoCrW alloys depended mostly on microstructural change and precipitates behavior; the tensile elongation increased with the reduction of

precipitates and the disappearance of diamond-like structure.

3. The large precipitates were associated with the increase of metal release; less amount of metal release can clearly occurred at the CoCrW alloys containing most ε phase without the precipitates. Therefore, the massive large precipitates were detrimental to the metal release.
4. The proper heat treatment can realize a promising high-strength and tensile ductility As-SLM CoCrW alloys while obtained acceptable the amount of metal release.

Acknowledgments

This work was financially supported by National Pilot Projects (No. XDA09020301). The authors also thank Senior Engineer Dr. Qiqiang Chen for ICP-AES test and analysis.

REFERENCES

Anissian, L., Stark, A., Dahlstrand, H., Granberg, B., Good, V., Bucht, E., 2002. Cobalt ions influence proliferation and function of human osteoblast-like cells. Acta Orthop. 73, 369–374.

Barucca, G., Santecchia, E., Majni, G., Girardin, E., Bassoli, E., Denti, L., Gatto, A., Iuliano, L., Moskalewicz, T., Mengucci, P., 2015. SLM Structural characterization of biomedical Co–Cr–Mo components produced by direct metal laser sintering. Mater. Sci. Eng. C Mater. Biol. Appl. 48, 263–269.

Bettini, E., Leygraf, C., Lin, C., Liu, P., Pan, J., 2012. Influence of grain boundaries on dissolution behavior of a biomedical CoCrMo Alloy: in-situ electrochemical-optical, AFM and SEM/TEM studies. J. Electrochem. Soc. 159, C422–C427.

Chen, Y., Li, Y., Kurosu, S., Yamanaka, K., Tang, N., Koizumi, Y., Chiba, A., 2014. Effects of sigma phase and carbide on the wear behavior of CoCrMo alloys in Hanks' solution. Wear 310, 51–62.

Dobbs, H., Robertson, J., 1983. Heat treatment of cast Co-Cr-Mo for orthopaedic implant use. J. Mater. Sci. 18, 391–401.

Fleury, C., Petit, A., Mwale, F., Antoniou, J., Zukor, D.J., Tabrizian, M., Huk, O.L., 2006. Effect of cobalt and chromium ions on human MG-63 osteoblasts in vitro: morphology, cytotoxicity, and oxidative stress. Biomaterials 27, 3351–3360.

Geurtsen, W., 2002. Biocompatibility of dental casting alloys. Crit. Rev. Oral Biol. Med. 13, 71–84.

Hedberg, Y., Odnevall Wallinder, I., 2014. Metal release and speciation of released chromium from a biomedical CoCrMo alloy into simulated physiologically relevant solutions. J. Biomed. Mater. Res. Part B: Appl. Biomater. 102, 693–699.

Hedberg, Y.S., Qian, B., Shen, Z., Virtanen, S., Wallinder, I.O., 2014. In vitro biocompatibility of CoCrMo dental alloys fabricated by selective laser melting. Dent. Mater. 30, 525–534.

Huang, P., Lopez, H., 1999. Athermal ε-martensite in a Co–Cr–Mo alloy: grain size effects. Mater. Lett. 39, 249–253.

Jacobs, J.J., Gilbert, J.L., Urban, R.M., 1998. Current concepts review-corrosion of metal orthopaedic implants. J. Bone Jt. Surg. 80, 268–282.

Koizumi, Y., Suzuki, S., Yamanaka, K., Lee, B.-S., Sato, K., Li, Y., Kurosu, S., Matsumoto, H., Chiba, A., 2013. Strain-induced martensitic transformation near twin boundaries in a biomedical Co–Cr–Mo alloy with negative stacking fault energy. Acta Mater. 61, 1648–1661.

López, H.F., Saldivar-Garcia, A.J., 2007. Martensitic transformation in a cast Co-Cr-Mo-C alloy. Metall. Mater. Trans. A 39, 8–18.

Lashgari, H.R., Zangeneh, S., Hasanabadi, F., Saghafi, M., 2010. Microstructural evolution during isothermal aging and strain-induced transformation followed by isothermal aging in Co–Cr–Mo–C alloy: a comparative study. Mater. Sci. Eng.: A 527, 4082–4091.

Lee, S.-H., Nomura, N., Chiba, A., 2007. Effect of Fe addition on microstructures and mechanical properties of Ni- and C-free Co–Cr–Mo alloys. Mater. Trans. 48, 2207–2211.

Lee, S.-H., Takahashi, E., Nomura, N., Chiba, A., 2005. Effect of heat treatment on microstructure and mechanical properties of Ni-and C-free Co–Cr–Mo alloys for medical applications. Mater. Trans. 46, 1790–1793.

Liao, Y., Pourzal, R., Stemmer, P., Wimmer, M., Jacobs, J., Fischer, A., Marks, L., 2012. New insights into hard phases of CoCrMo metal-on-metal hip replacements. J. Mech. Behav. Biomed. Mater. 12, 39–49.

Liu, F., Lin, X., Yang, G., Song, M., Chen, J., Huang, W., 2011. Microstructure and residual stress of laser rapid formed Inconel 718 nickel-base superalloy. Opt. Laser Technol. 43, 208–213.

Lu, Y., Wu, S., Gan, Y., Li, J., Zhao, C., Zhuo, D., Lin, J., 2015. Investigation on the microstructure, mechanical property and corrosion behavior of the selective laser melted CoCrW alloy for dental application. Mater. Sci. Eng.: C 49, 517–525.

Matsumoto, H., Koizumi, Y., Ohashi, T., Lee, B.-S., Li, Y., Chiba, A., 2014. Microscopic mechanism of plastic deformation in a polycrystalline Co–Cr–Mo alloy with a single hcp phase. Acta Mater. 64, 1–11.

Mazur, M., Kalisz, M., Wojcieszak, D., Grobelny, M., Mazur, P., Kaczmarek, D., Domaradzki, J., 2015. Determination of structural, mechanical and corrosion properties of Nb_2O_5 and $(Nb_yCu_{1-y})O_x$ thin films deposited on Ti_6Al_4V alloy substrates for dental implant applications. Mater. Sci. Eng. C Mater. Biol. Appl. 47, 211–221.

Mitsunobu, T., Koizumi, Y., Lee, B.-S., Yamanaka, K., Matsumoto, H., Li, Y., Chiba, A., 2014. Role of strain-induced martensitic transformation on extrusion and intrusion formation during fatigue deformation of biomedical Co–Cr–Mo–N alloys. Acta Mater. 81, 377–385.

Mori, M., Yamanaka, K., Kuramoto, K., Ohmura, K., Ashino, T., Chiba, A., 2015. Effect of carbon on the microstructure, mechanical properties and metal ion release of Ni-free Co–Cr–Mo alloys containing nitrogen. Mater. Sci. Eng.: C 55, 145–154.

Mori, M., Yamanaka, K., Matsumoto, H., Chiba, A., 2010. Evolution of cold-rolled microstructures of biomedical Co–Cr–Mo alloys with and without N doping. Mater. Sci. Eng.: A 528, 614–621.

Narushima, T., Mineta, S., Kurihara, Y., Ueda, K., 2013. Precipitates in biomedical Co–Cr alloys. JOM 65, 489–504.

Okazaki, Y., Gotoh, E., 2005. Comparison of metal release from various metallic biomaterials in vitro. Biomaterials 26, 11–21.

Okazaki, Y., Gotoh, E., 2008. Metal release from stainless steel, Co–Cr–Mo–Ni–Fe and Ni–Ti alloys in vascular implants. Corros. Sci. 50, 3429–3438.

Okazaki, Y., Tateishi, T., Ito, Y., 1997. Corrosion resistance of implant alloys in pseudo physiological solution and role of alloying elements in passive films. Mater. Trans. JIM 38, 78–84.

Patel, B., Favaro, G., Inam, F., Reece, M.J., Angadji, A., Bonfield, W., Huang, J., Edirisinghe, M., 2012. Cobalt-based orthopaedic alloys: relationship between forming route, microstructure and tribological performance. Mater. Sci. Eng.: C 32, 1222–1229.

Rosenthal, R., Cardoso, B.R., Bott, I.S., Paranhos, R.P.R., Carvalho, E.A., 2010. Phase characterization in as-cast F–75 Co–Cr–Mo–C alloy. J. Mater. Sci. 45, 4021–4028.

Saldivar-Garcia, A., Lopez, H., 2004. Temperature effects on the lattice constants and crystal structure of a Co–27Cr–5Mo low-carbon alloy. Metall. Mater. Trans. A 35, 2517–2523.

Songür, M., Çelikkan, H., Gökmeşe, F., Şimşek, S.A., Altun, N.Ş., Aksu, M.L., 2009. Electrochemical corrosion properties of metal alloys used in orthopaedic implants. J. Appl. Electrochem. 39, 1259–1265.

Summer, B., Fink, U., Zeller, R., Rueff, F., Maier, S., Roider, G., Thomas, P., 2007. Patch test reactivity to a cobalt–chromium–molybdenum alloy and stainless steel in metal-allergic patients in correlation to the metal ion release. Contact Dermat. 57, 35–39.

Sun, S.-H., Koizumi, Y., Kurosu, S., Li, Y.-P., Matsumoto, H., Chiba, A., 2014. Build direction dependence of microstructure and high-temperature tensile property of Co–Cr–Mo alloy fabricated by electron beam melting. Acta Mater. 64, 154–168.

Takaichi, A., Suyalatu, Nakamoto, T., Joko, N., Nomura, N., Tsutsumi, Y., Migita, S., Doi, H., Kurosu, S., Chiba, A., Wakabayashi, N., Igarashi, Y., Hanawa, T., 2013. Microstructures and mechanical properties of Co–29Cr–6Mo alloy fabricated by selective laser melting process for dental applications. J. Mech. Behav. Biomed. Mater. 21, 67–76.

van der Voet, G.B., Todorov, T.I., Centeno, J.A., Jonas, W., Ives, J., Mullick, F.G., 2007. Metals and health: a clinical toxicological perspective on tungsten and review of the literature. Mil. Med. 172, 1002–1005.

Yamanaka, K., Mori, M., Chiba, A., 2011. Mechanical properties of as-forged Ni-free Co–29Cr–6Mo alloys with ultrafine-grained microstructure. Mater. Sci. Eng.: A 528, 5961–5966.

Yamanaka, K., Mori, M., Chiba, A., 2014a. Dynamic recrystallization of a biomedical Co–Cr–W-based alloy under hot deformation. Mater. Sci. Eng.: A 592, 173–181.

Yamanaka, K., Mori, M., Chiba, A., 2014b. Effects of carbon concentration on microstructure and mechanical properties of as-cast nickel-free Co–28Cr–9 W-based dental alloys. Mater. Sci. Eng.: C 40, 127–134.

Yamanaka, K., Mori, M., Chiba, A., 2014c. Effects of nitrogen on microstructural evolution of biomedical Co–Cr–W alloys during hot deformation and subsequent cooling. Mater. Des. 57, 421–425.

Yamanaka, K., Mori, M., Chiba, A., 2014d. Refinement of solidification microstructures by carbon addition in biomedical Co–28Cr–9W–1Si alloys. Mater. Lett. 116, 82–85.

Yamanaka, K., Mori, M., Chiba, A., 2014e. Influence of carbon addition on mechanical properties and microstructures of Ni-free Co–Cr–W alloys subjected to thermomechanical processing. J. Mech. Behav. Biomed. Mater. 37, 274–285.

Yamanaka, K., Mori, M., Kuramoto, K., Chiba, A., 2014f. Development of new Co–Cr–W-based biomedical alloys: Effects of microalloying and thermomechanical processing on microstructures and mechanical properties. Mater. Des. 55, 987–998.

Yoda, K., Suyalatu, Takaichi, A., Nomura, N., Tsutsumi, Y., Doi, H., Kurosu, S., Chiba, A., Igarashi, Y., Hanawa, T., 2012. Effects of chromium and nitrogen content on the microstructures and mechanical properties of as-cast Co–Cr–Mo alloys for dental applications. Acta Biomater. 8, 2856–2862.

Zangeneh, S., Lashgari, H.R., Roshani, A., 2012. Microstructure and tribological characteristics of aged Co–28Cr–5Mo–0.3C alloy. Mater. Design. 37, 292–303.

Zhang, J., Gao, L., Cui, L., Wang, H., Yang, J., 2005. Analysis in the variation principle of thermal cycle and stress in the laser overlapping area. Laser. Technol. 4, 370–372.

Zhang, X., Li, Y., Tang, N., Onodera, E., Chiba, A., 2014. Corrosion behaviour of CoCrMo alloys in 2 wt% sulphuric acid solution. Electrochim. Acta 125, 543–555.